Submitted for Publication
Nuclear Physics

Cross Sections and Complex Phase Shifts for the Scattering of Protons from ^{12}C at the 8.20 MeV and 9.14 MeV Anomalies†

J. B. Swint††, J. S. Duval, Jr., A. C. L. Barnard
and
T. B. Clegg†††

T. W. Bonner Nuclear Laboratories, Rice University
Houston, Texas

Abstract

Absolute differential cross sections as a function of angle for the elastic scattering of protons from ^{12}C and for the inelastic scattering reaction $^{12}C(p,p')^{12}C^*$ (Q = -4.43 MeV) were measured at incident proton energies E_p = 8.20, 9.100, 9.113, 9.121, 9.127, 9.130, 9.138, 9.150, 9.160, 9.201, 9.222, and 9.264 MeV. Complex phase shifts were obtained to represent the elastic scattering cross sections and the total inelastic cross sections. The complex phase shift analysis has confirmed the $J^\pi = 3/2^-$ assignment at the 8.20 MeV anomaly and $7/2^-$ for the stronger state at the 9.14 MeV double anomaly. The weaker state of the doublet, which is the lower in energy, has $J^\pi = 5/2^-$, confirming the assignment by Terrell and Bernstein. These assignments were used in a calculation which reproduced the features of the elastic scattering cross sections as a function of energy over the 9.14 MeV doublet. An examination of the behaviour of the phase shifts over the anomaly revealed that the total phase shift for the $f_{5/2}$ partial wave does not pass through 90° whereas the total phase shift for the $f_{7/2}$ partial wave does pass through 90°.

---

† Supported by the U. S. Atomic Energy Commission

†† Now at the University of Florida, Gainesville, Florida.

††† National Aeronautics and Space Administration Fellow in Physics; now at the University of Wisconsin, Madison, Wisconsin.

I. Introduction

In a recent paper[1] it was reported that the well-known anomaly at 9.14 MeV in the elastic scattering of protons from ^{12}C is caused by more than one state in ^{13}N. The present paper reports measurements made at eleven energies over this anomaly, and also at one energy at the 8.20 MeV anomaly.

When the complex structure of the 9.14 MeV anomaly was first observed, it was presumed that two levels were involved: the $7/2^-$ state previously associated with this anomaly and the $9/2^+$ state predicted by shell model calculations[2] but not seen experimentally. Extensive efforts were made to fit the data with these assumptions, but without success. Other positive-parity assignments to the second state were also unsuccessful. Recently Terrell and Bernstein[3] suggested that the second state had $J = 5/2^-$, and the assumption of a strong $7/2^-$ state and a weaker $5/2^-$ state has produced good fits to the data. Since the weaker state does not appear in conventional p-shell calculations[2], it is presumed due to two-nucleon excitation into higher shells.

It has been reported[4] that the total phase shift for the $d_{3/2}$ partial wave over the 5.37 MeV anomaly in the elastic scattering of protons from ^{12}C does not pass through 90°. In the present experiment this phenomenon has been observed for the $f_{5/2}$ partial wave over the 9.14 MeV anomaly in the elastic scattering of protons from ^{12}C.

II. Experimental Methods and Results

The experimental methods were exactly as described previously[1,4]. Angular distributions for the elastic scattering and for the inelastic scattering reaction $^{12}C(p,p')^{12}C^*$ (Q = -4.43 MeV) were measured at incident energies E_p = 8.20, 9.100, 9.113, 9.121, 9.127, 9.130, 9.138, 9.150, 9.160, 9.201, 9.222, and 9.264 MeV. The data at the lowest energy are shown in fig. 1 and at the higher energies in figs. 2 and 3. The r.m.s. errors are estimated as 4% for the inelastic cross sections. Fig. 4 shows elastic cross sections at fixed angles as a function of energy over the 9.14 MeV anomaly, taken

from reference 1). Fig. 5 shows the cross section as a function of energy with arrows to indicate the energies at which the angular distributions were taken.

A Legendre series has been fitted to the inelastic scattering angular distributions and the necessary coefficients are shown in table 1, together with the total cross sections implied. The Legendre series are plotted as solid curves on figs. 1 and 3.

III. Phase Shift Analysis

The complex phase shifts which represent the elastic scattering angular distributions and the total inelastic cross sections were obtained by the method previously described[5] and are shown in table 2. The angular distributions calculated from the complex phase shifts appear as solid and dashed curves on figs. 1 and 2, and are in excellent agreement with the experimental data. The phase shifts indicate that the $5/2^-$ state lies below the $7/2^-$ state in energy. The nonresonant phase shifts in table 2 agree quite well with those at nearby energies[5]. Fig. 6 shows the partial scattering amplitudes for the $f_{5/2}$ and $f_{7/2}$ partial waves in the complex plane and demonstrates graphically the behaviour of the phase shifts over the 9.14 MeV anomaly. Fig. 8 shows the phase shifts for the $f_{5/2}$ and $f_{7/2}$ partial waves as a function of energy over the 9.14 MeV anomaly.

IV. Calculation of Cross Sections as a Continuous Function of Energy

The diagonal elements of the collision matrix were approximated by[5]

$$U_\ell^J(E) = \left[\alpha_\ell^J \exp(2i\delta_\ell^J)\right]\left\{1 + \alpha_\ell^J\left[\exp(2i\beta_\ell^J) - 1\right]\right\}$$

where the term outside the square parentheses describes the processes varying slowly with energy and the inside term describes rapidly varying processes due to single level in the compound nucleus. The values of the slowly varying parameters were chosen to agree with table 2 and reference 5), and the rapidly varying

parameter $\underline{\beta}$ was taken to have the usual energy dependence close to a narrow level: $\beta(E) = \text{arc tg } \frac{\Gamma(E)}{2(E_o - E)}$. The partial width $\underline{a}$ was taken to be a constant for a particular level.

Using these expressions, cross sections were calculated as a function of energy over the 9.14 MeV anomaly and are shown in fig. 4. The parameters used for the two states are shown in table 3. It can be seen that the features of the experimental data have been reproduced by the calculation.

V. Discussion

As mentioned in the introduction it was found by the authors that the data over the 9.14 MeV anomaly could not be reproduced by a $J^\pi = 7/2^-$ state and a positive-parity state. However, the assignment $J^\pi = 5/2^-$ to the second state, first suggested to the authors by Terrell and Bernstein[3], has been found to be consistent with the data and is viewed with confidence. It can be seen from fig. 3 that the inelastic angular distributions do not change dramatically over the doublet, and in particular that the signs of the coefficients of the Legendre polynomials P_1, P_3, and P_5 remain the same. Thus these terms must be due to interference between a resonant state and a nonresonant background of opposite parity. Since interference between a $7/2^-$ state and a $3/2^+$ background gives rise to a pure P_3 term, the coefficient of the P_3 term in the inelastic scattering angular distributions is presumed due to interference between the $7/2^-$ state and the tail of the very broad $3/2^+$ state at 6.6 MeV. Interference between a $5/2^-$ state and a $3/2^+$ background is characterized by a strong P_1 term. It can be seen from table 1 that the P_1 coefficient is anomalous near the resonance energy of the weaker state. Fig. 4 demonstrates that the $5/2^- - 7/2^-$ assignment is consistent with the elastic scattering data. Thus both the elastic and inelastic scattering data are consistent with the $5/2^-$ assignment. The polarization data and cross sections of Terrell and Bernstein[3] are similarly consistent with this assignment.

In Kurath's calculations[2] of the negative parity states of ^{13}N, all possible states for a given number of nucleons in the 1-p shell are formed. No $5/2^-$ state appears with excitation energy in the 10 MeV region. However, Kurath notes that excitation of two nucleons from the 1-p shell to the 1-d shell would give

higher lying negative parity states. The $5/2^-$ state is presumed to be one of these

VI. Acknowledgements

The authors gratefully acknowledge discussions with Dr. Glen Terrell, who originated the $J^\pi = 5/2^-$ assignment.

References

1. J. B. Swint, A. C. L. Barnard, T. B. Clegg and J. L. Weil, Nuclear Physics,
2. D. Kurath, Phys. Rev. 101 (1956) 216;
   D. Kurath and R. D. Lawson, Nuclear Physics 23 (1961) 5;
   D. Kurath, private communication
3. G. Terrell and E. M. Bernstein, private communication
4. J. S. Duval, Jr., A. C. L. Barnard and J. B. Swint, Nuclear Physics, to be published
5. A. C. L. Barnard, J. B. Swint and T. B. Clegg, Nuclear Physics

Figure Captions

Figure 1 Absolute differential cross sections for the elastic scattering of protons by ^{12}C and the inelastic scattering reaction $^{12}C(p,p')^{12}C^*$ ($Q = -4.43$ MeV) as a function of angle at $E_p = 8.20$ MeV. The points are the experimental data. The dashed curve was calculated from the derived phase shifts in table 2, and the solid curve was calculated from the Legendre series in table 1. Note the elastic scattering cross sections have been displaced by 0.5 b/sr and the inelastic scattering cross sections have been multiplied by 10.

Figure 2a,b,c Absolute differential cross sections for the elastic scattering of protons by ^{12}C as a function of angle at the energies shown. The points are the experimental data, and the solid and dashed curves were calculated from the phase shifts in table 2. Note that the cross sections have been displaced by the amounts given in parentheses.

Figure 3a,b,c Absolute differential cross sections for the inelastic scattering reaction $^{12}C(p,p')^{12}C^*$ ($Q = -4.43$ MeV) as a function of angle at the energies shown. The points are the experimental data, and the solid curves were calculated from the Legendre series in table 1. Note the cross sections have been displaced by the amounts given in the parentheses

Figure 4 Absolute differential cross sections for the elastic scattering of protons by ^{12}C as a function of incident proton energy (lab system) at the angles shown (centre-of-mass system). The points are from ref. 1 and the solid curves were calculated as described in the text.

Figure Captions, continued

Figure 5 Absolute differential cross sections as a function of energy for the elastic scattering of protons by ^{12}C. The arrows in the figure indicate the energy positions of the angular distributions.

Figure 6a,b a) Partial scattering amplitude for the $f_{5/2}$ partial wave over the 9.14 MeV anomaly plotted in the complex plane. The points are the derived phase shifts in table 2. The solid line is a smooth curve drawn through the points.

b) Partial scattering amplitude for the $f_{7/2}$ partial wave over the 9.14 MeV anomaly plotted in the complex plane. The points are the derived phase shifts from table 2. The solid curve is a smooth curve drawn through the points.

Figure 7a,b a) Complex phase shifts for the $f_{5/2}$ partial wave over the 9.14 MeV anomaly. The points are the derived phase shifts in table 2, and the solid curve is a smooth curve drawn through the points.

b) Complex phase shifts for the $f_{7/2}$ partial wave over the 9.14 MeV anomaly. The points are the derived phase shifts in table 2, and the solid curve is a smooth curve drawn through the points.

Table 1

Coefficients of Legendre series which represent the $^{12}C(p,p')^{12}C$ data and the resulting total reaction cross sections.

E_p	A_0	A_1	A_2	A_3	A_4	A_5	A_6	CHISQ	σ_T(mb)
9.100	0.0255	-0.0021	0.0134	-0.0087	-0.0066	0.0022	0.0022	0.0003	320
9.113	0.0249	-0.0008	0.0150	-0.0084	-0.0044	0.0019	0.0039	0.0004	313
9.121	0.0257	-0.0024	0.0140	-0.0096	-0.0053	0.0009	0.0033	0.0002	323
9.127	0.0283	-0.0036	0.0169	-0.0070	-0.0016	0.0051	0.0062	0.0019	355
9.130	0.0355	-0.0084	0.0077	-0.0200	-0.0065	0.0077	0.0054	0.0007	445
9.138	0.0317	-0.0068	0.0088	-0.0219	-0.0091	0.0006	0.0042	0.0005	398
9.150	0.0383	-0.0036	0.0031	-0.0196	-0.0105	0.0053	0.0068	0.0005	480
9.160	0.0445	-0.0032	-0.0003	-0.0254	-0.0103	0.0079	0.0110	0.0001	559
9.201	0.0288	-0.0037	0.0095	-0.0093	-0.0071	0.0073	0.0043	0.0005	362
9.222	0.0239	-0.0032	0.0082	-0.0060	-0.0064	0.0034	0.0014	0.0007	300
9.264	0.0215	-0.0013	0.0097	0.00004	-0.0059	0.0031	0.0020	0.0004	270

Table 2

Complex phase shifts which represent the data

	E_p	Δ_0 / A_0	Δ_1^+ / A_1^+	Δ_1^- / A_1^-	Δ_2^+ / A_2^+	Δ_2^- / A_2^-	Δ_3^+ / A_3^+	Δ_3^- / A_3^-	χ
a	9.100	71.00	-14.17	-35.00	-14.00	148.00	38.50	5.86	.0809
		0.83	0.95	0.75	0.76	0.74	0.88	0.92	
b	9.113	71.50	-14.50	-35.00	-14.50	146.60	38.00	180.00	.0864
		0.84	0.95	0.75	0.76	0.73	1.00	0.59	
c	9.121	71.50	-14.50	-35.00	-14.50	146.12	38.00	174.36	.0524
		0.84	0.95	0.75	0.76	0.72	0.99	0.46	
d	9.127	71.00	-14.00	-35.00	-14.50	145.00	42.02	171.65	.0365
		0.84	0.95	0.75	0.76	0.74	0.98	0.49	
e	9.130	71.00	-13.80	-35.00	-15.39	150.80	53.78	160.00	.0579
		0.85	0.95	0.74	0.76	0.73	0.82	0.59	
f	9.138	72.00	-14.00	-35.00	-14.50	149.00	48.93	170.97	.0469
		0.84	0.95	0.75	0.76	0.74	0.92	0.56	
g	9.150	71.00	-13.60	-35.00	-16.00	151.00	81.13	159.93	.0679
		0.85	0.95	0.75	0.73	0.70	0.62	0.59	
h	9.160	72.00	-14.00	-35.00	-14.00	152.50	86.50	157.07	.0702
		0.83	0.95	0.76	0.72	0.73	0.35	0.93	
i	9.201	71.94	-16.00	-38.00	-13.00	148.00	141.78	165.00	.1114
		0.87	0.93	0.77	0.70	0.76	0.37	1.00	
j	9.222	72.00	-15.60	-37.00	-13.32	148.00	173.28	158.11	.0885
		0.84	0.97	0.77	0.76	0.70	0.40	1.00	
k	9.264	73.00	-13.00	-37.00	-13.80	148.56	4.07	160.40	.0715
		0.84	0.95	0.75	0.72	0.72	0.60	1.00	

Table 3

Level Parameters in ^{13}N

E_p (MeV)	J^π	$\Gamma(E_p)$ (keV)	Δ_ℓ^J
9.145	$5/2^-$	12	0.28
9.152	$7/2^-$	90	0.75

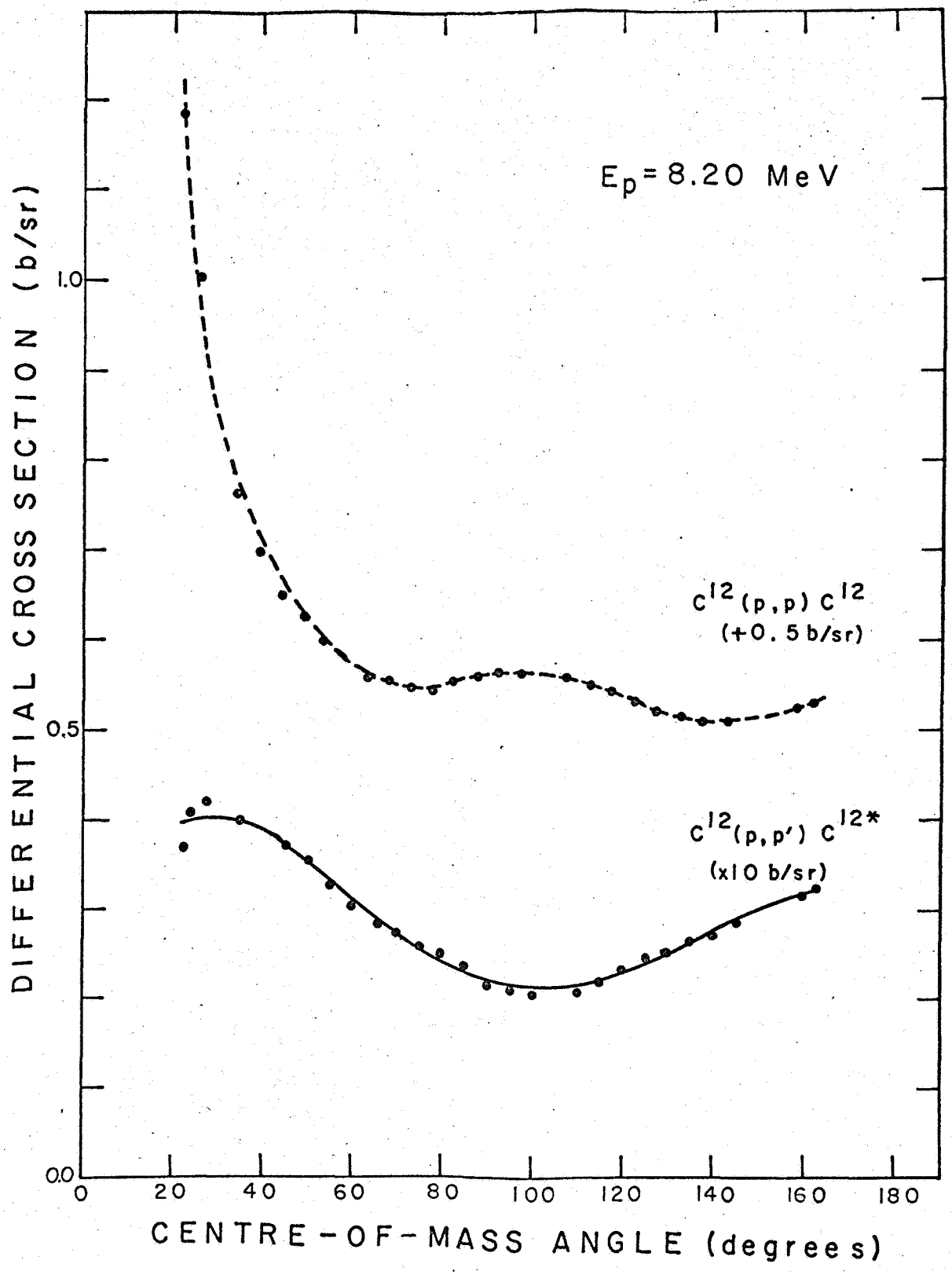
E_p = 8.20 MeV
$C^{12}(p,p)\,C^{12}$
(+0.5 b/sr)
$C^{12}(p,p')\,C^{12*}$
(x10 b/sr)
DIFFERENTIAL CROSS SECTION (b/sr)
1.0
0.5
0.0
0
20
40
60
80
100
120
140
160
180
CENTRE-OF-MASS ANGLE (degrees)

FIG. 1

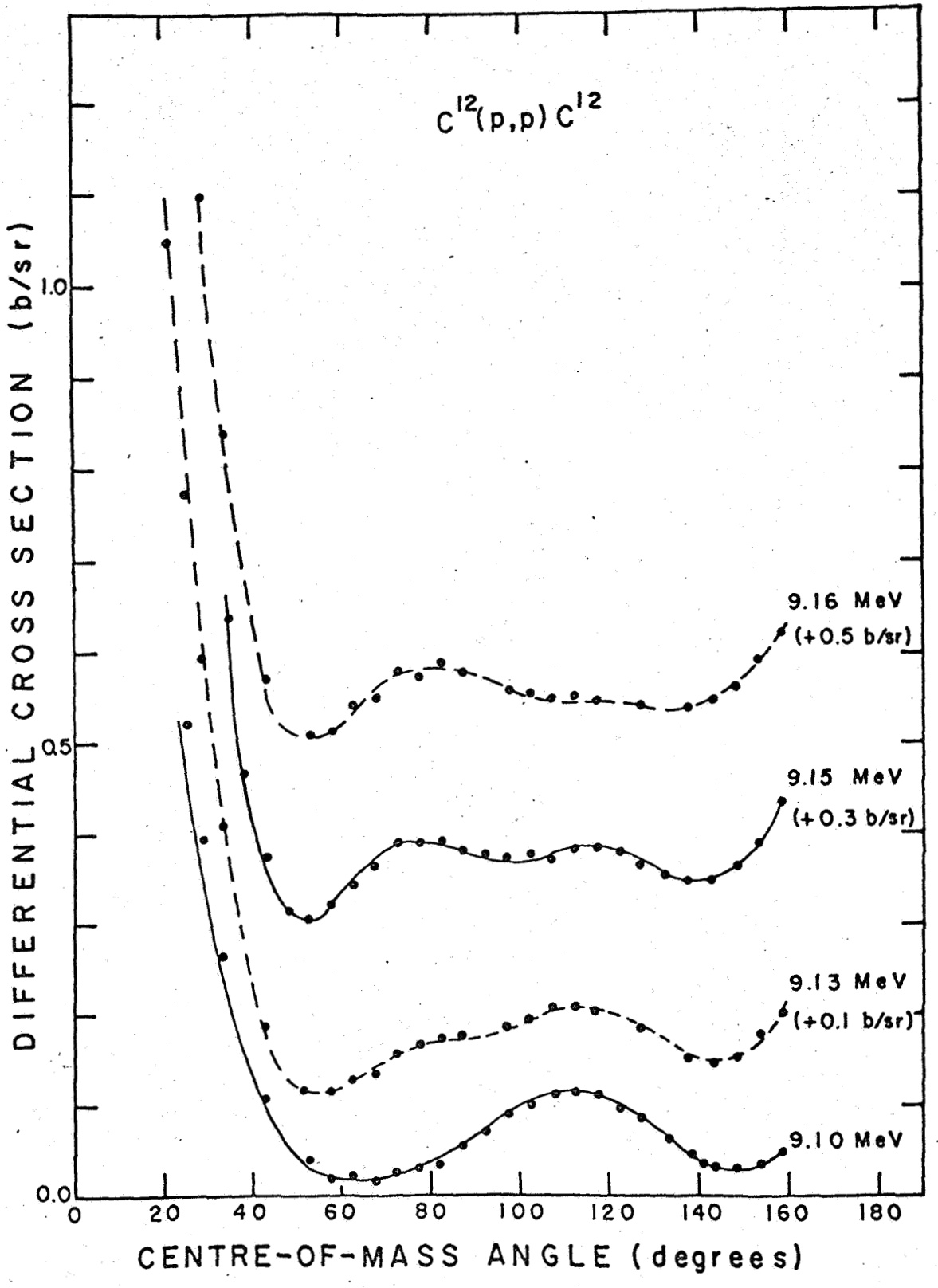
$C^{12}(p,p)C^{12}$
DIFFERENTIAL CROSS SECTION (b/sr)
1.0
0.5
0.0
9.16 MeV
(+0.5 b/sr)
9.15 MeV
(+0.3 b/sr)
9.13 MeV
(+0.1 b/sr)
9.10 MeV
0
20
40
60
80
100
120
140
160
180
CENTRE-OF-MASS ANGLE (degrees)

FIG. 2 a

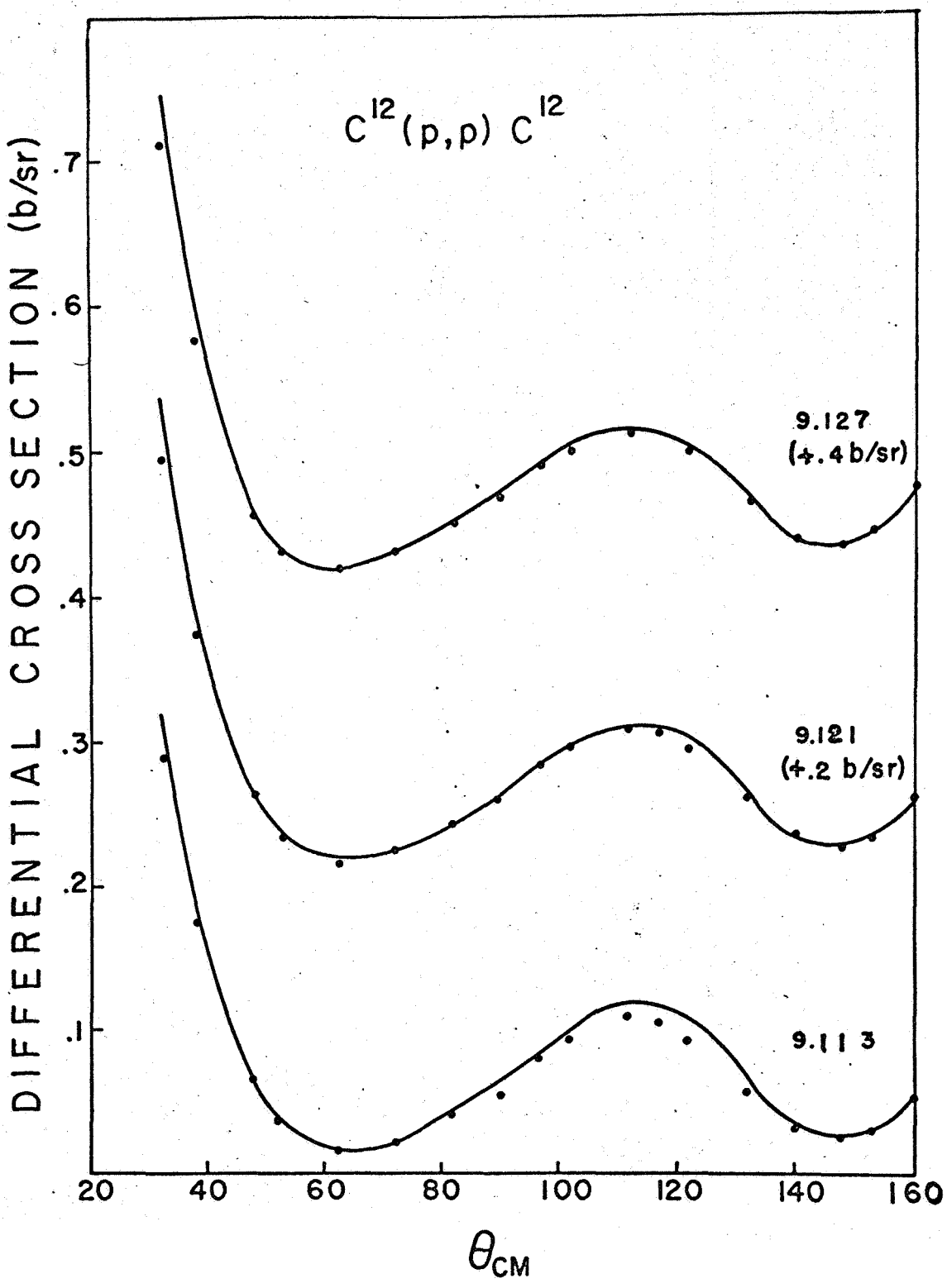
$C^{12}(p,p)\ C^{12}$
DIFFERENTIAL CROSS SECTION (b/sr)
.7
.6
.5
.4
.3
.2
.1
9.127
(4.4 b/sr)
9.121
(4.2 b/sr)
9.113
20
40
60
80
100
120
140
160
θ_{CM}

FIG. 2 b

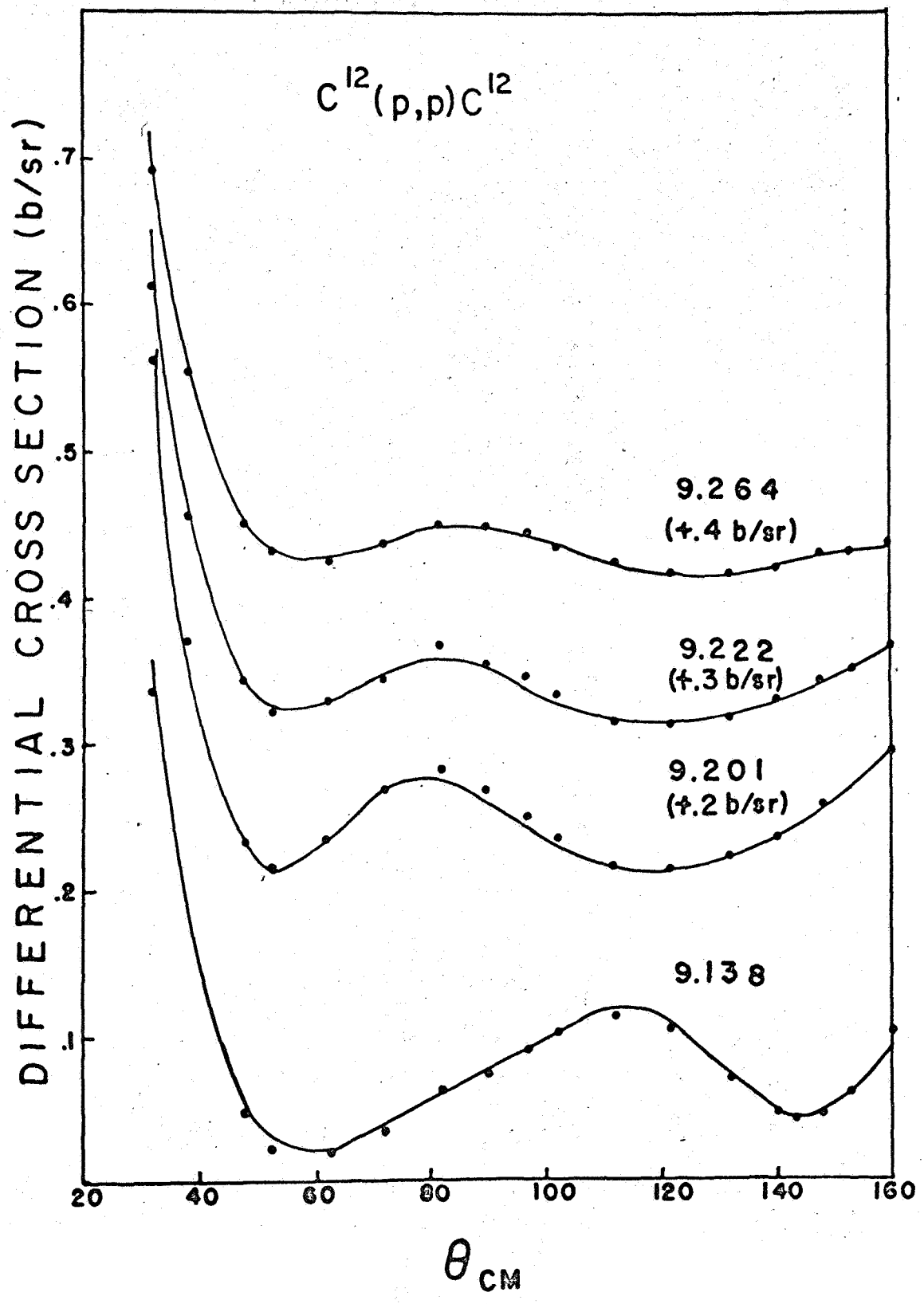
$C^{12}(p,p)C^{12}$
DIFFERENTIAL CROSS SECTION (b/sr)
.7
.6
.5
.4
.3
.2
.1
9.264
(+.4 b/sr)
9.222
(+.3 b/sr)
9.201
(+.2 b/sr)
9.138
20
40
60
80
100
120
140
160
θ_{CM}

FIG. 2 c

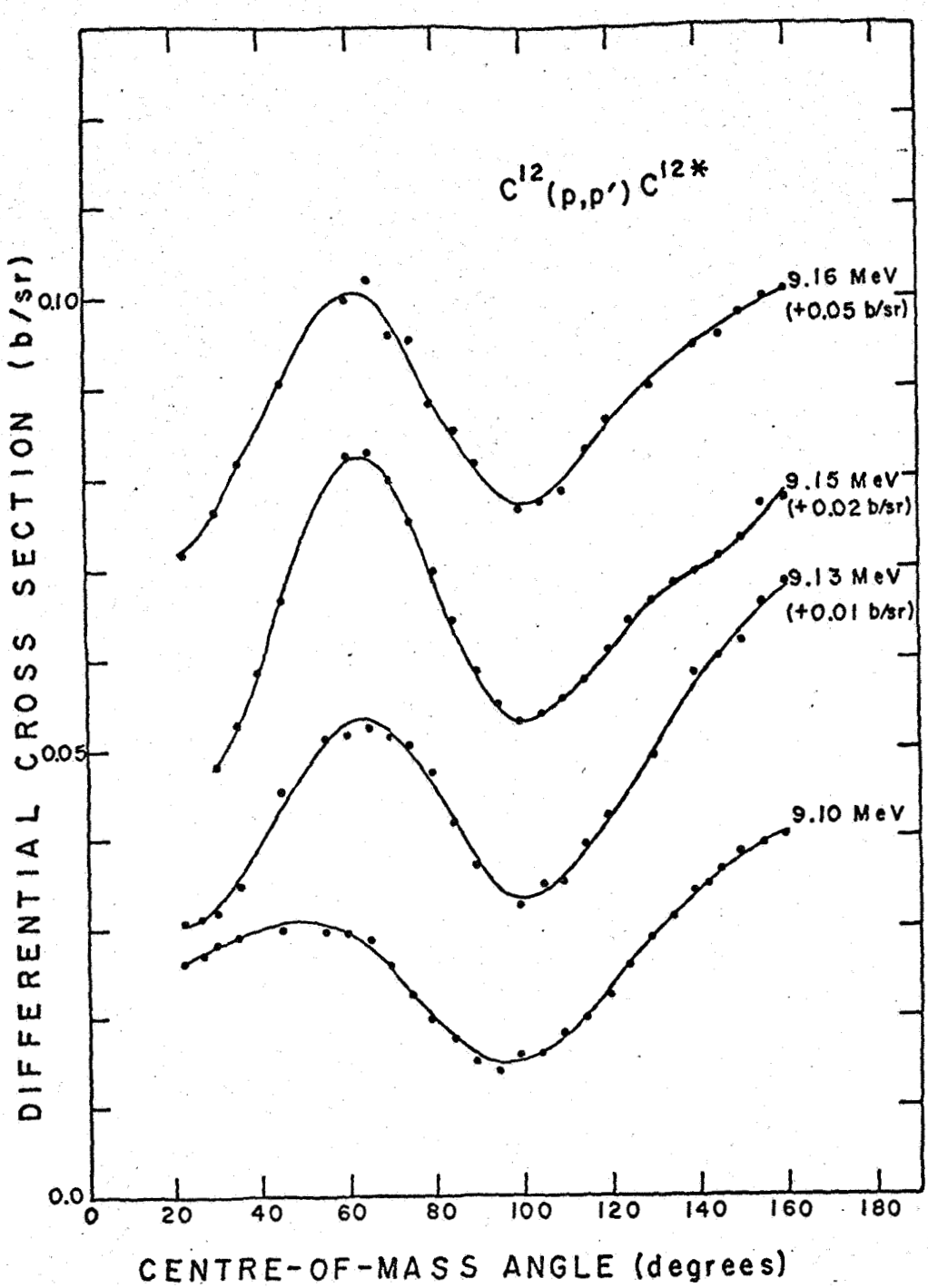
$C^{12}(p,p')C^{12*}$
9.16 MeV
(+0.05 b/sr)
9.15 MeV
(+0.02 b/sr)
9.13 MeV
(+0.01 b/sr)
9.10 MeV
DIFFERENTIAL CROSS SECTION (b/sr)
0.10
0.05
0.0
0
20
40
60
80
100
120
140
160
180
CENTRE-OF-MASS ANGLE (degrees)

FIG. 3*a*

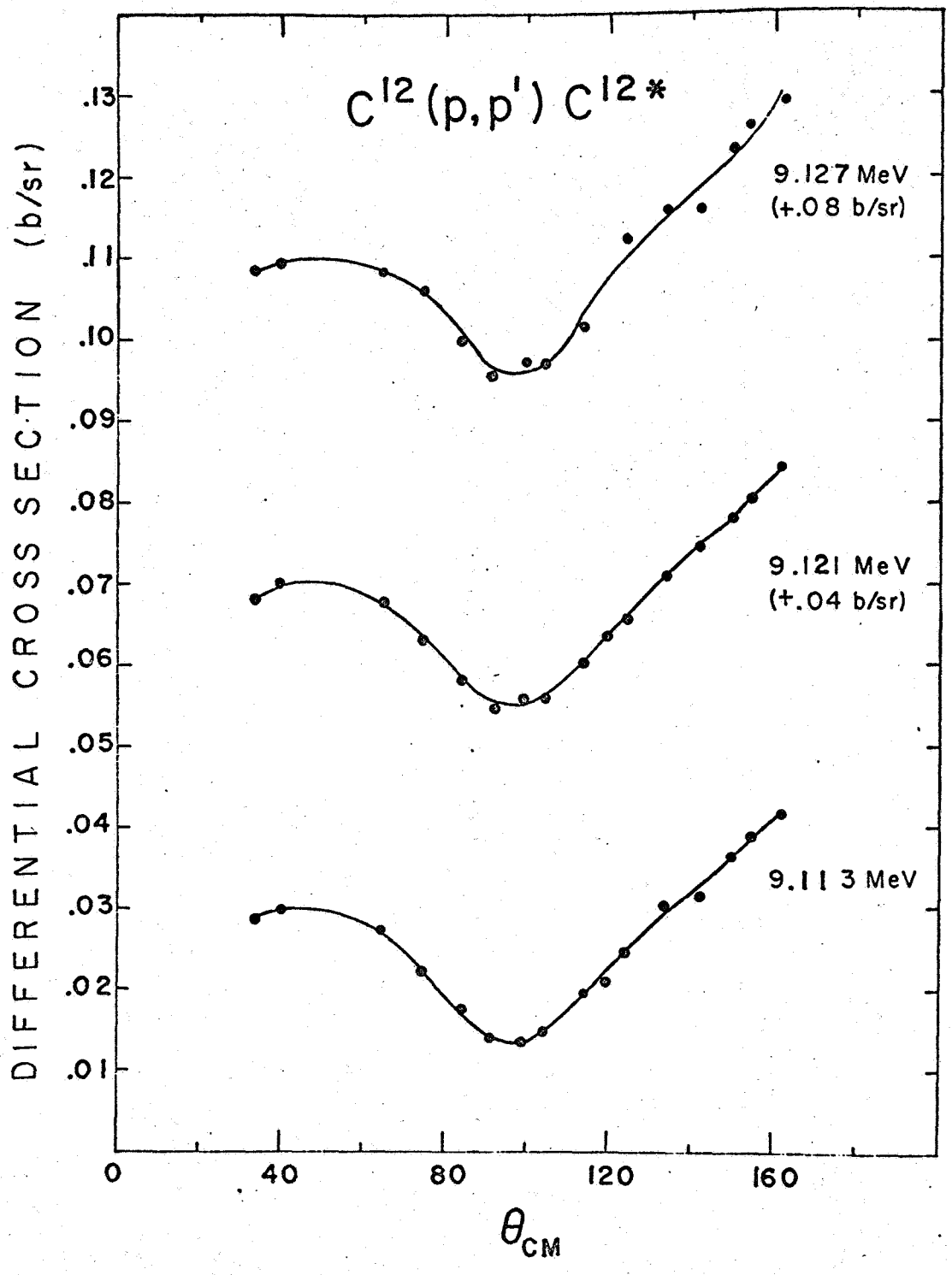
$C^{12}(p,p')\,C^{12*}$
9.127 MeV
(+.08 b/sr)
9.121 MeV
(+.04 b/sr)
9.113 MeV
DIFFERENTIAL CROSS SECTION (b/sr)
.13
.12
.11
.10
.09
.08
.07
.06
.05
.04
.03
.02
.01
0
40
80
120
160
θ_{CM}

FIG. 3b

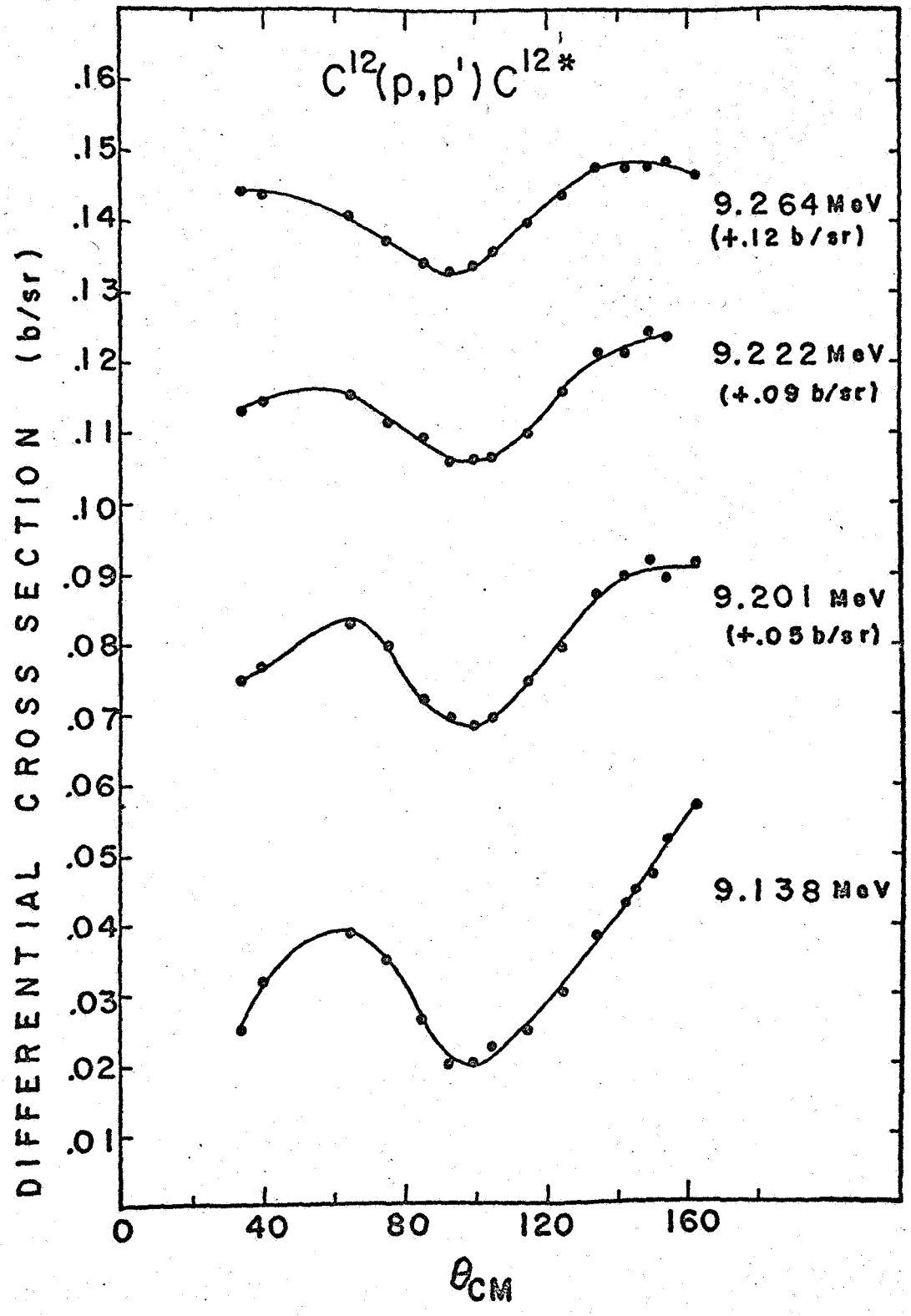
$C^{12}(p,p')C^{12*}$
9.264 MeV
(+.12 b/sr)
9.222 MeV
(+.09 b/sr)
9.201 MeV
(+.05 b/sr)
9.138 MeV
DIFFERENTIAL CROSS SECTION (b/sr)
.16
.15
.14
.13
.12
.11
.10
.09
.08
.07
.06
.05
.04
.03
.02
.01
0
40
80
120
160
θ_{CM}

FIG. 3c

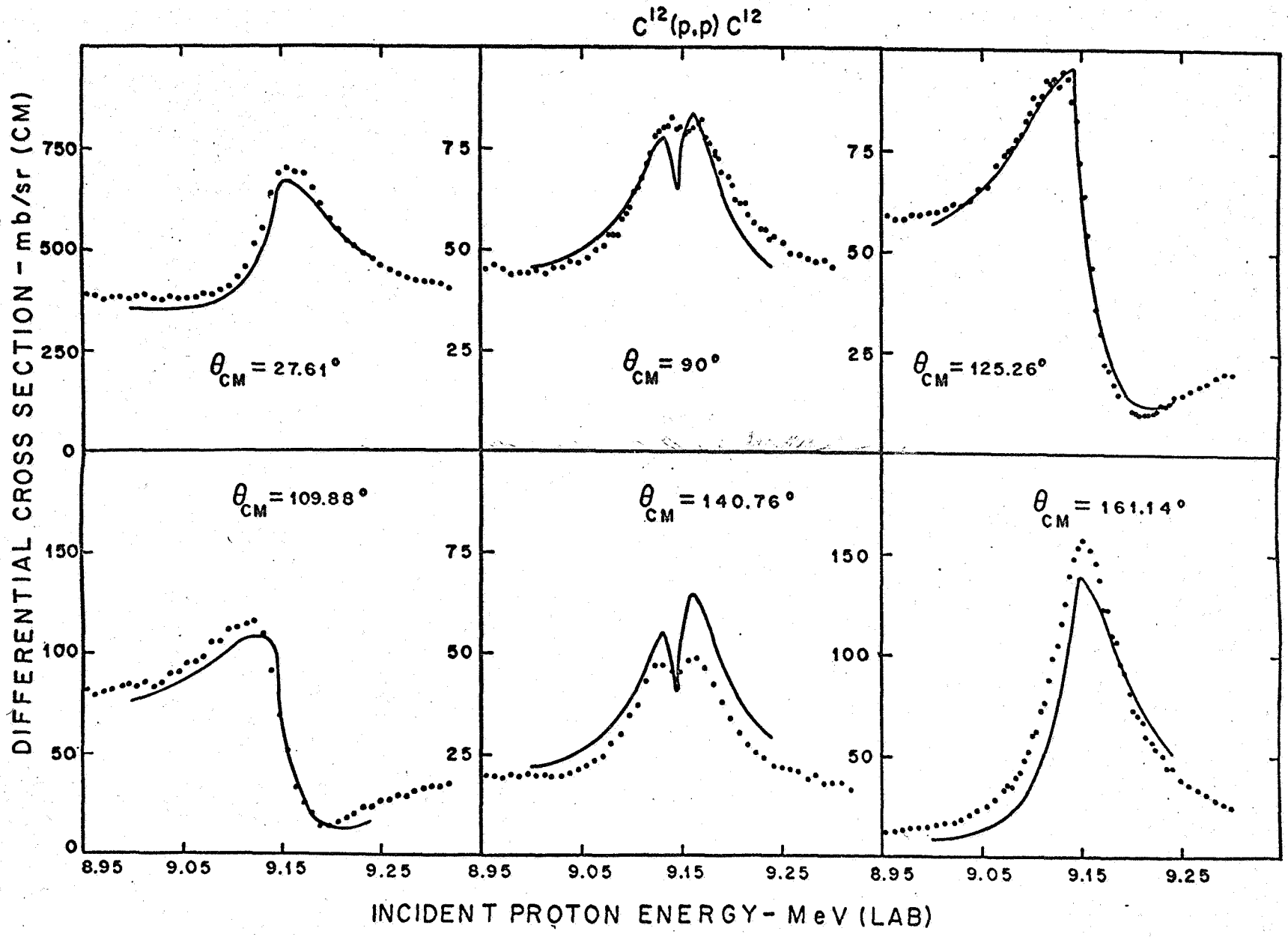
C12(p,p) C12
DIFFERENTIAL CROSS SECTION - mb/sr (CM)
INCIDENT PROTON ENERGY - MeV (LAB)
θCM = 27.61°
θCM = 90°
θCM = 125.26°
θCM = 109.88°
θCM = 140.76°
θCM = 161.14°
8.95
9.05
9.15
9.25

FIG. 4

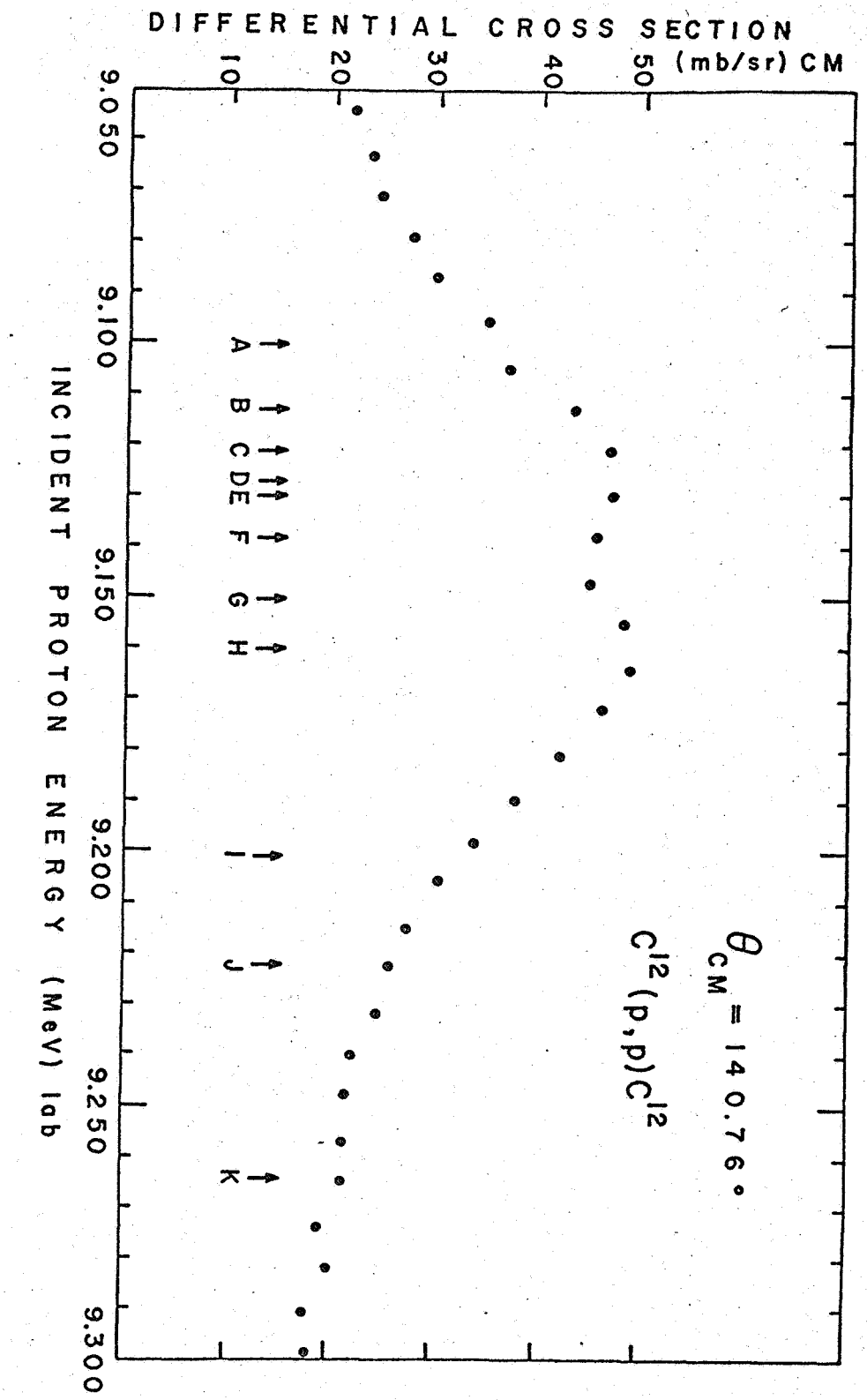
DIFFERENTIAL CROSS SECTION
(mb/sr) CM
10
20
30
40
50
9.050
9.100
9.150
9.200
9.250
9.300
INCIDENT PROTON ENERGY (MeV) lab
A
B
C
D
E
F
G
H
I
J
K
$\theta_{CM} = 140.76°$
$C^{12}(p,p)C^{12}$

FIG. 5

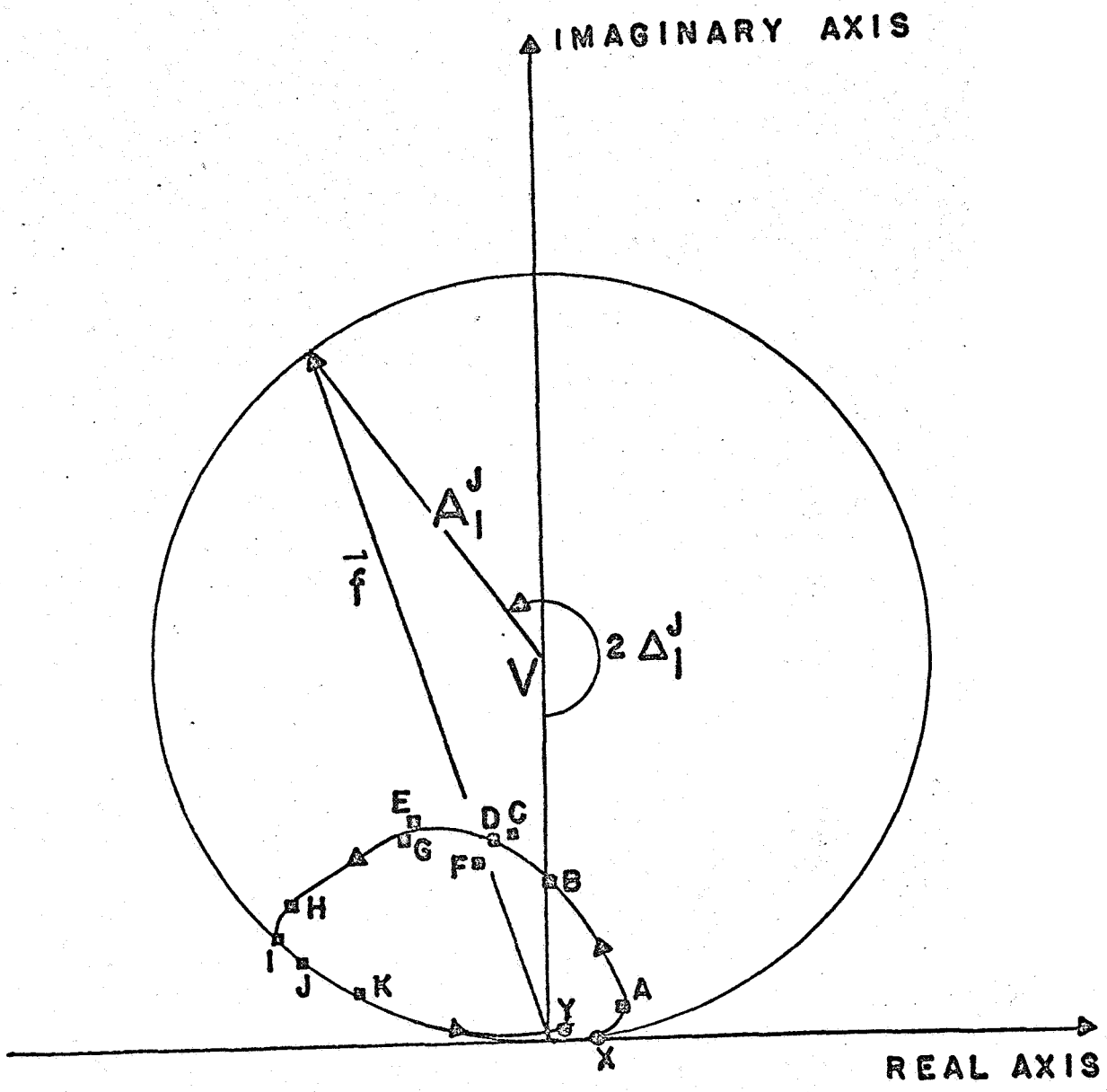
IMAGINARY AXIS
Δ_1^J
$\vec{f}$
V
$2\Delta_1^J$
E
D
C
G
F
B
H
I
J
K
A
Y
X
REAL AXIS

FIG. 6a

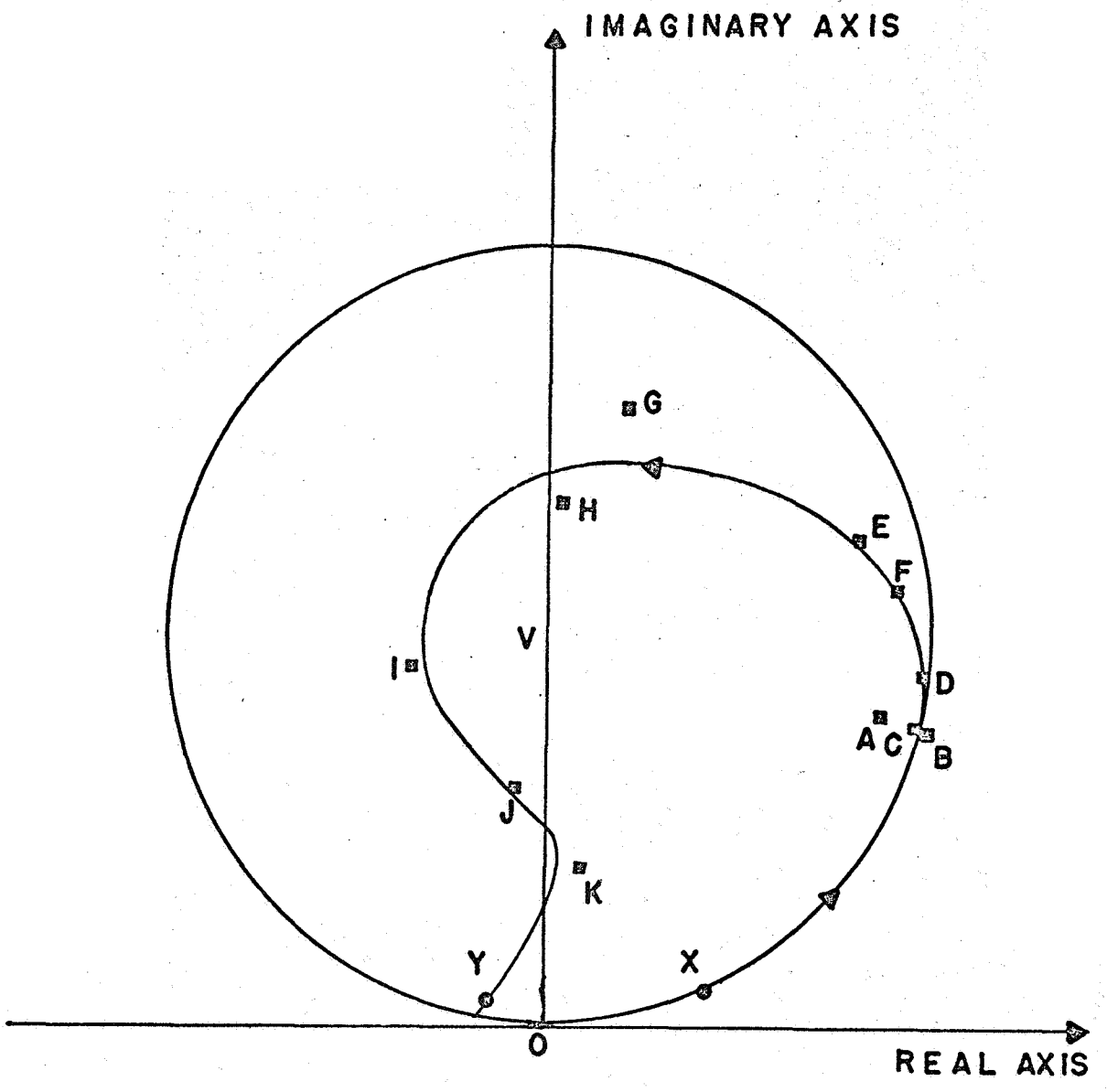

FIG. 6b

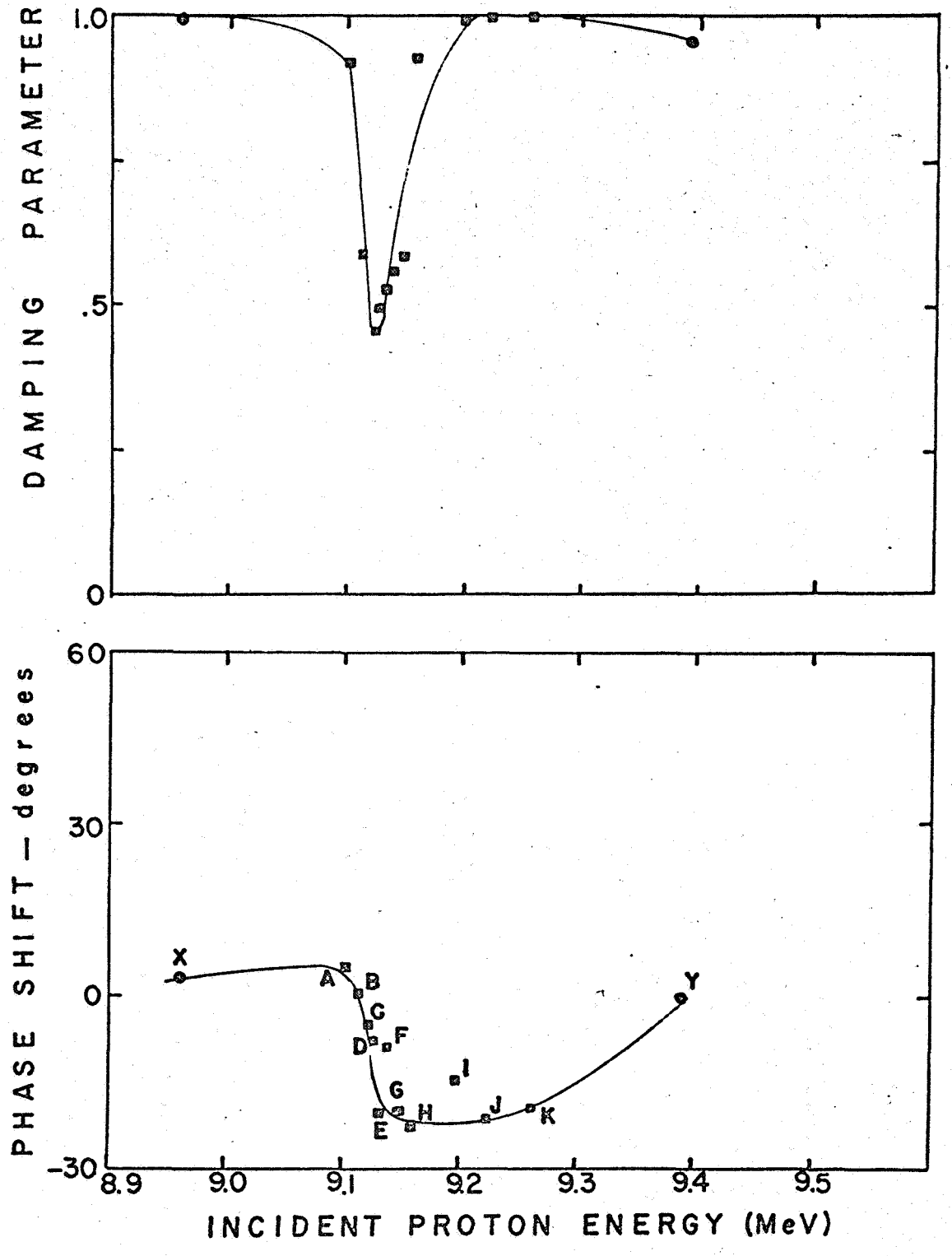
DAMPING PARAMETER
1.0
.5
0
PHASE SHIFT — degrees
60
30
0
-30
X
A
B
C
D
E
F
G
H
I
J
K
Y
8.9
9.0
9.1
9.2
9.3
9.4
9.5
INCIDENT PROTON ENERGY (MeV)

FIG. 7a

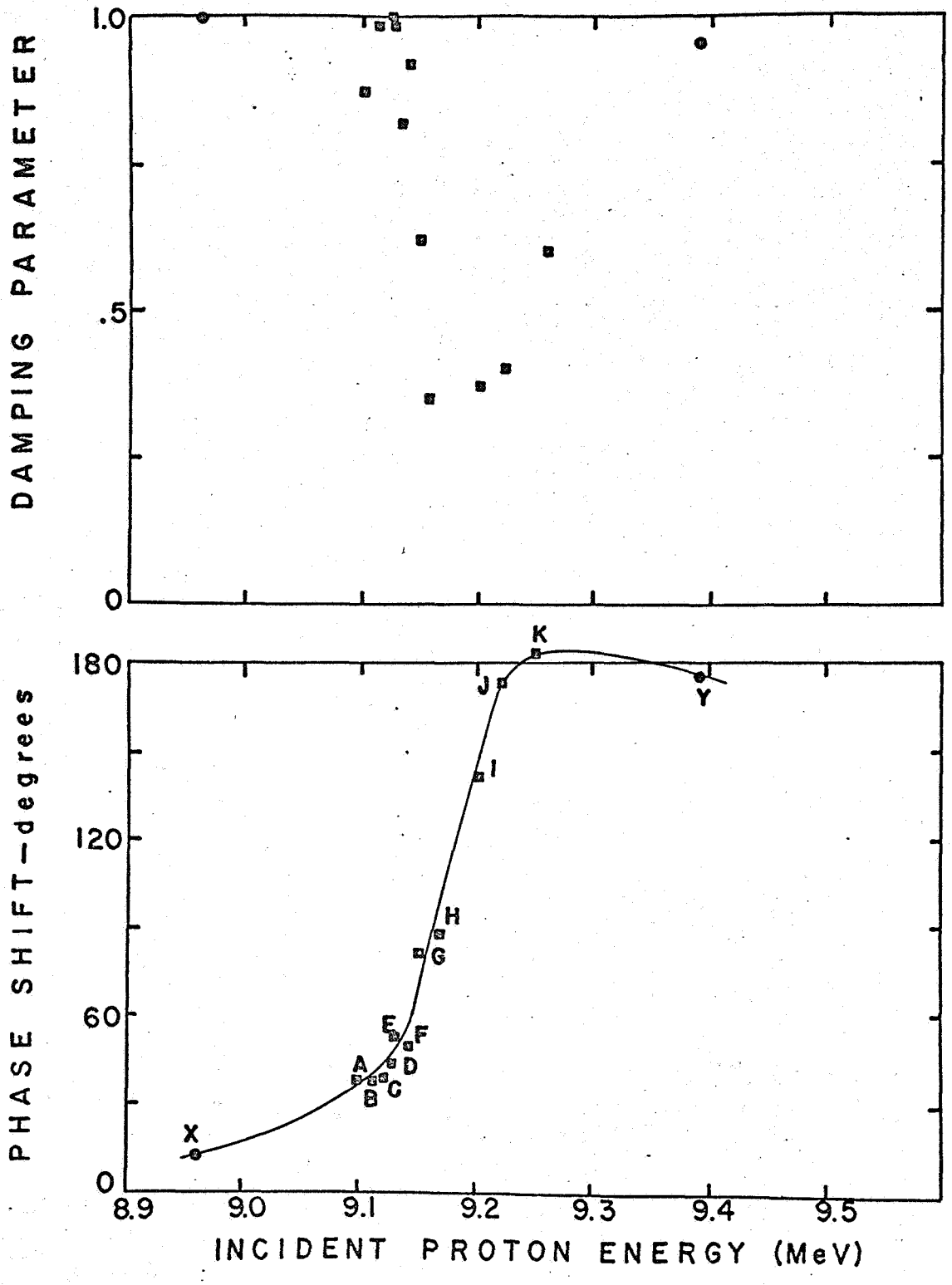
DAMPING PARAMETER
1.0
.5
0
PHASE SHIFT—degrees
180
120
60
0
8.9
9.0
9.1
9.2
9.3
9.4
9.5
INCIDENT PROTON ENERGY (MeV)
X
A
B
C
D
E
F
G
H
I
J
K
Y

FIG. 7 b